Ullah, Kaleem; García-Cámara, Braulio; Habib, Muhammad; Yadav, N.P.; Liu, Xuefeng. (2018) An indirect method of imaging the Stokes parameters of a submicron particle with sub-diffraction scattering, *Journal of Quantitative Spectroscopy and Radiative Transfer*, v. 213, pp.: 35-40.

DOI: https://doi.org/10.1016/j.jqsrt.2018.04.015

An Indirect Method of Imaging the Stokes Parameters of a Submicron Particle with Sub-diffraction Scattering

Kaleem Ullah[1], Braulio Garcia-Camara[2], Muhammad Habib[3], N.P. Yadav[1] and Xuefeng Liu[1, *]

[1]*School of electronic Engineering and Optoelectronic Technology, Nanjing University of Science and Technology, Nanjing, 210094, Jiangsu, China*

[2]*Group of Displays and Photonic Applications (GDAF-UC3M). Carlos III University of Madrid, Leganes, 28911 Madrid, Spain*

[3]*National Synchrotron Radiation Lab, University of Science and Technology of China, Hefei, Anhui, China*

*kaleem758@gmail.com

Abstract

In this work, we report an indirect way to image the Stokes parameters of a sample under test (SUT) with sub-diffraction scattering information. We apply our previously reported technique called parametric indirect microscopic imaging (PIMI) based on a fitting and filtration process to measure the Stokes parameters of a submicron particle. A comparison with a classical Stokes measurement is also shown. By modulating the incident field in a precise way, fitting and filtration process at each pixel of the detector in PIMI make us enable to resolve and sense the scattering information of SUT and map them in terms of the Stokes parameters. We believe that our finding can be very useful in fields like singular optics, optical nanoantenna, biomedicine and much more. The spatial signature of the Stokes parameters given by our method has been confirmed with finite difference time domain (FDTD) method.

Keywords: Sub-diffraction, polarization modulation, scattering, Stokes parameters.

1. Introduction

In any conventional optical far-field microscopy, when the light is focused by the objective lens, a blurry spot is formed due to diffraction [1,2]. The width of this light spot can be calculated through the Rayleigh limit. This establishes that the radius of the spot is given by 0.6λ/NA, where NA is the numerical aperture of the lens and λ is the wavelength of the incident wavelength [3-8]. Numerous approaches have been used to break this diffraction barrier. Several of them achieved a

lateral resolution of tens of nanometers, substantially lower than the wavelength of light, but each with its own limitations [9–16]. A continuous effort to develop existing and new techniques is needed to harness the benefits of optical far field microscopy for ultra-resolution imaging. The foundation of the super-resolution of an optical microscopy depends on the detection of the near field signals which contains the sub-wavelength features of the sample under test (SUT) [17,18]. It is true that near field scanning optical microscopy (NSOM) can collect the near field information by scanning with a sharp tip, a few nanometer away from the SUT, forming an image which is beyond the diffraction limit [19–22]. However, NSOM is difficult to operate in non-invasive mode and only limited to the surface imaging [23]. Furthermore, its mapping area with subwavelength features is narrow. Recently, proposed super and hyper-lens can also achieve nanoscale scattering features by using the evanescent wave spectrum in a clever way [24]. However, a subsequent study demonstrated that resolving capability of the super-lens is seriously weaken by the material losses, related to the resonant nature of the enhanced evanescent waves. Furthermore, evanescent waves could not be focused by using the conventional optics [24–28].

Stokes parameters are used to describe both the optical response and the polarization state of the SUT. Therefore, Stokes parameters with sub-diffraction scattering signals are desired in many applications, such as nano-fabrication [29], optical nanoantenna [30], surface plasmon excitation [31], optical data transmission [32] and so on. Several methods have been reported in the literature to measure the Stokes parameters. Among these methods, some of them are really simple [33,34], some are using tightly focused beams [35] and meta-lenses [36] to map the Stokes parameters with subwavelength scattering distributions. These reported simple methods do not provide a high-sensitivity of Stokes imaging [33, 34], and those techniques which are highly sensitive are not simple and cost effective [36]. The objective of applying our technique is to provide a platform to measure the Stokes parameters with sub-diffraction scattering distribution using a cost effective and simple system. We confirm the high sensitivity of our system by comparing it with a conventional far field microscopy and also with FDTD simulations.

Sub-wavelength anisotropic features in the SUT produces variations in the far-field scattering, which come from a near-field to far-field coupling. Our PIMI system [37] uses a polarization modulation illumination scheme to obtained these far field scattering changes. In particular, changes arising in the far-field point spread function (PSF) are produced due to this

coupling effect because different polarization illumination collects different scattering information. After filtering and fitting at each pixel, the PSF becomes narrow, giving rise to the resolution smaller than the wavelength [37]. In other words, we can map the nanoscale scattering distribution of the SUT. In this work, we report the ability of PIMI technique to image the Stokes parameters of an isolated submicron particle with sub-diffraction scattering distribution. A comparison with the Stokes parameters measured by a classical method is also included to show the relevant differences and the strength of this technique. The spatial signatures of the Stokes parameters delivered by PIMI have been also verified by FDTD simulations.

2. Theoretical and Experimental Basis

2.1 Stokes Parameters Measurement by Classical Method

In the traditional way, the measurement of the Stokes parameters can be carried out with the help of two optical components named as retarder and polarizer [38]. The first three Stokes parameters can be calculated by rotating the transmission axis of the polarizer, whereas for finding the last Stokes parameter, i.e. S_3, a retarder is required to convert the linearly polarized light into left or right circularly polarized light [33, 39]. Figure 1 shows the schematic representation of the measurement of the Stokes parameters as well as a scheme of the calculation of each parameter and the polarization configurations. The first Stokes parameter, S_0, represents the total intensity whereas the second one, S_1, quantifies a difference in the intensities in x and y, providing information on a linear polarization as shown in Fig. 1(b). S_2 measured the difference of two electric field components at diagonal positions [40], i.e. 45° and 135°, as shown in Fig. 1(b). The last parameter, S_3, illustrates the difference between left and right circularly polarized [38] measured by positioning a quarter wave-plate at 45° and 135° in the optical path of the optical system, as it is shown in Fig. 1(a).

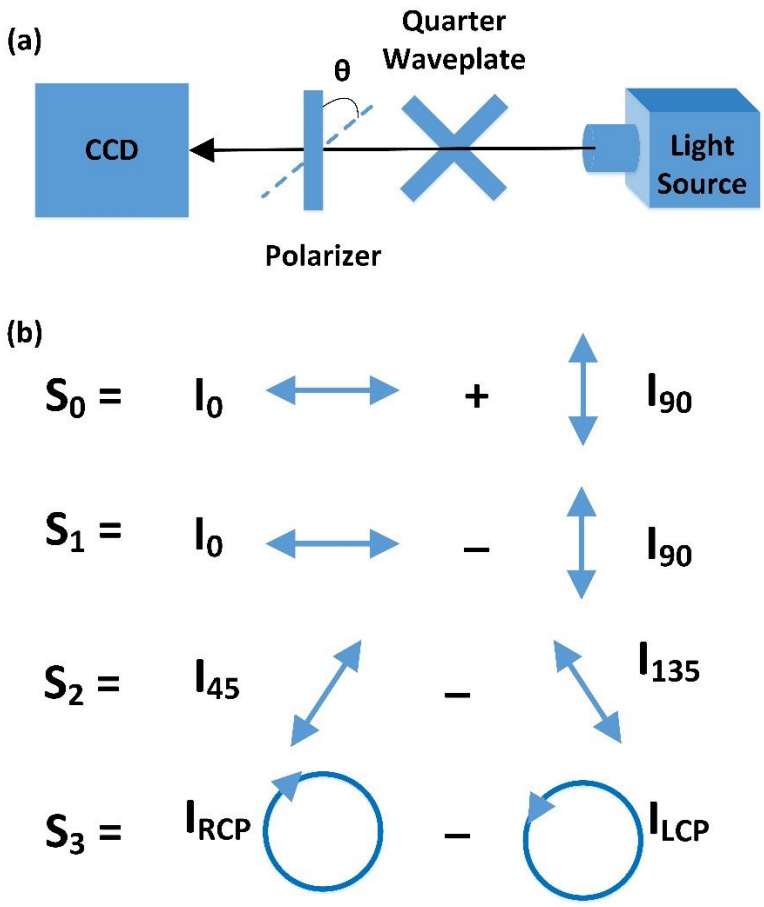

Figure 1. (a) Schematic of the classical measurement setup of the Stokes parameters. (b) A representation of the Stokes parameters in the form of polarization pattern displayed as arrows and four equations.

2.2 Stokes Parameters Measurement by PIMI Method

PIMI system is built by modifying a conventional optical far field microscopy such that the variation of the polarization status of incident light can be precisely controlled. When this linear polarized beam with different polarization angles impinges on the SUT, it collects different information depending on the atomic arrangement of the SUT. A schematic of the PIMI system is displayed in Figure 2(a) (see Methods section for further information). A Cu_2O submicron sphere is considered as sample to be probed. Its scanning electron microscopy image has been displayed in Fig. 2(b) to check its spherical shape and estimate its size (diameter ~ 900 nm). The scattering

field distribution for a complete incident polarization angle range has been shown in Fig. 2(d). As can be observed, the scattering spatial distribution is changed for every polarization. This change arises due to the directionality of the atomic or molecular arrangements. This variation of the refractive index with the direction of the vibration of the light is represented by a surface called indicatrix [41]. It has a general form of ellipse [41], as can be seen in Fig. 2(c). For any general direction of the light, an elliptical cross-section of the indicatrix is observed and optical anisotropy is given by the difference in the length of the elliptical axis [41].

In PIMI, we rotated the incident linearly polarized light from 0^o to 360^o before impinging on the SUT with a period angle of 18^o. Therefore, the detector intensity follows a sine wave cycleso, we can formulate the intensity variation at each spatial point covered by the PSF by using the Jones Model [41]. The experimental spatial points which follow the fitting criteria (*Adj. Root Square* = 90) [37] fit well with the reconstruction curve as shown in Fig. 3(a) and they are regarded as the fitting points or the authentic points. On the other hand, those spatial points which are below this merit criteria are considered as noise and filtered out [37]. Figure 3 shows the fitting and filtration process followed by PIMI technique. The filtering process has been illustrated in Fig 3(b), the points whose *Adj. R. Square* value is larger than 90 follows the reconstruction curve as shown in Fig. 3(a), whereas, the points do not reach this criteria filtered out as noise as can be visualized from Fig. 3(b). Only the central points of the PSF at each pixel follows the near to far field coupling principle and fulfills the fitting criteria. The points other than the central points of each pixel filters out and we can be able to differentiate between two close range points as can be seen from the Fig. 3(c, d). By removing the extra diffraction in each pixel of the CCD, the width of the PSF narrowed down and we can differentiate between two closely situated points as can be observed well from the Fig. 3(e). In other words, we can image the nanoscale field mapping in PIMI system which cannot be possible with the classical far field microscopy.

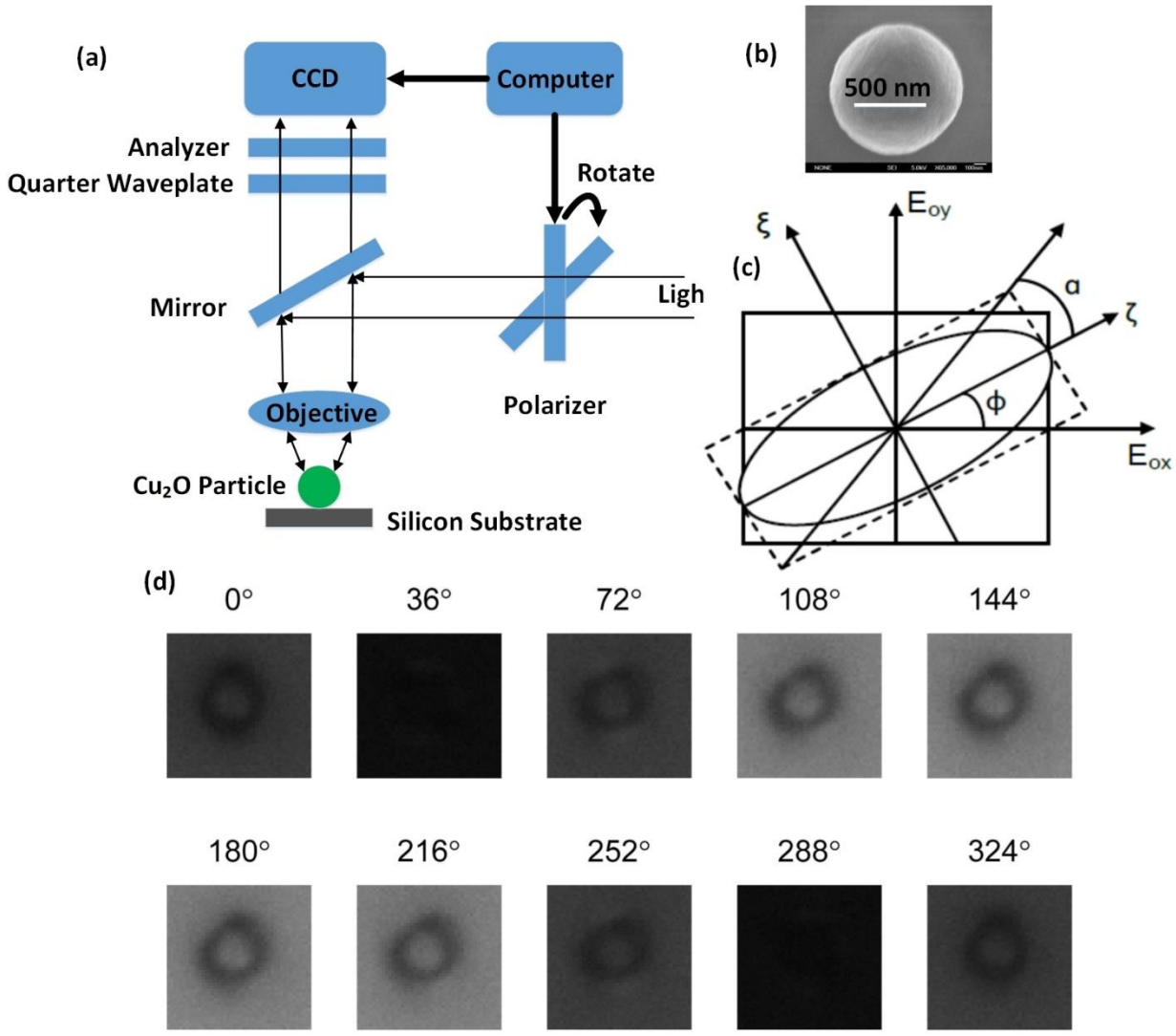

Figure 2. (a) Schematic of the PIMI system (b) The SEM image of the Cu_2O sphere. (c) Polarization ellipse representation where E_{0x} and E_{0y} are the horizontal and vertical components of the electric field, ϕ is the azimuthal angle along the slow vibration axis i.e. E_{0x} axis. (d) Intensity field images were taken by modulating the linear polarization light at a various angles range of 532 nm wavelength with 100x objective of 0.90 numerical aperture.

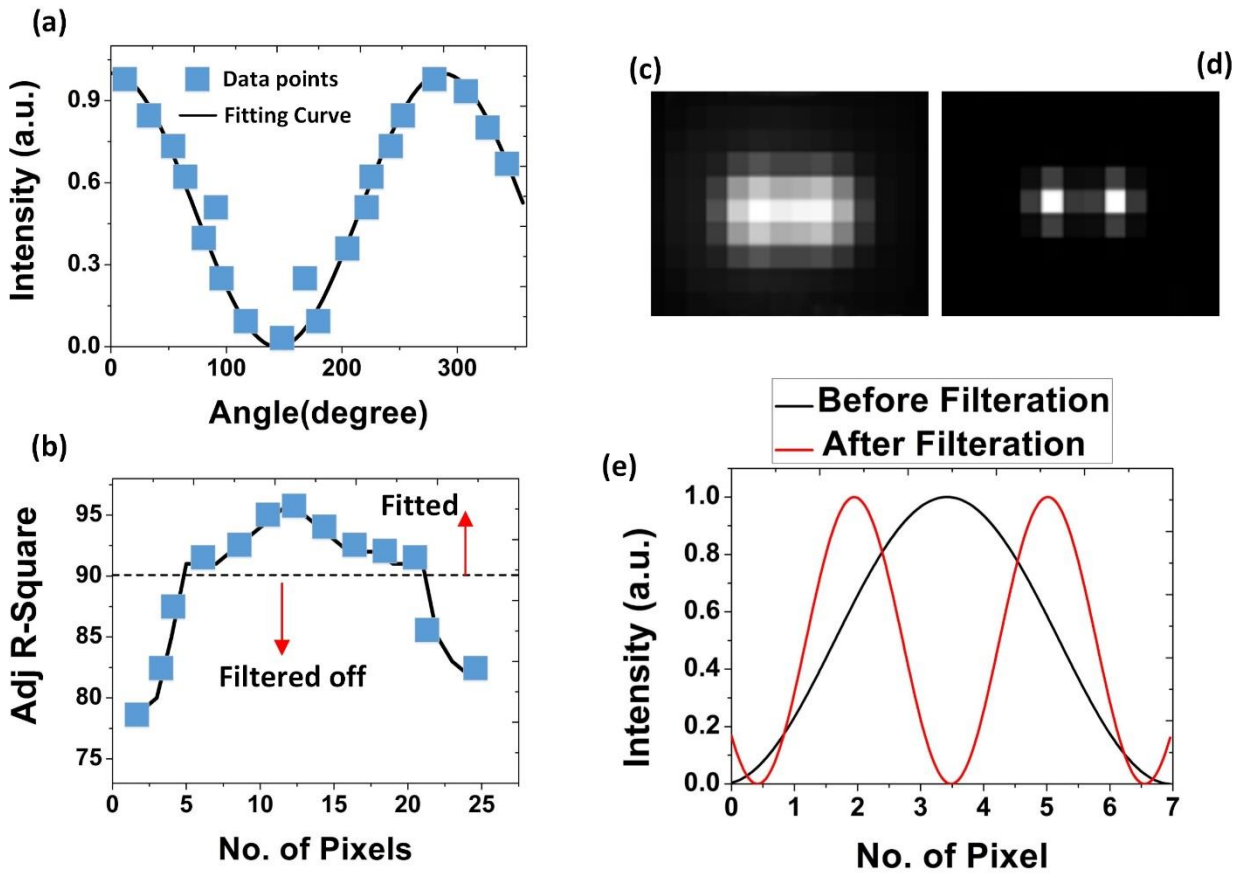

Figure 3. (a) A representation of the fitting the experimental data points. (b) The process of filtration shows how points which did not follow the equation 3 remove and how neighboring diffraction which is present in the conventional microscopic blurry spot (c) removed that helps us to distinguish between two close range points (d). (e) Intensity line graph by plotting the data extracted from (c, d) on the same position.

We rotate the linear polarization field from 0° to 360°, so, we can express the intensity of the complete modulation process as [41]·[42]:

$$I = \frac{I_0}{2}[1 + \sin 2(\alpha - \phi)\sin\delta] \qquad (1)$$

Where I_0 is the non-polarized intensity, α is the input polarization angle, ϕ is the angle along the slow vibration axis (see Fig. 1(c)) and δ is the optical retardation (the phase shift between the E_y and E_x). The field scattered distribution which has been displayed in Fig. 2(d) can be defined by

the equation 1. The lower and higher value of the intensity depends on the factor *sin2(a-ϕ)*. As shown in Fig. 2(d), the intensity of the polarization angle of 36° and 288° is minimum whereas the brighter intensity in case of the 108°, 144°, 180°, and 216° can be observed.

By expanding equation (1) trigonometrically, it can be obtained that:

$$I = \frac{1}{2} I_0 + \frac{1}{2} I_0 \sin\delta \cos 2\phi \sin 2\alpha + \frac{1}{2} I_0 \sin\delta \sin 2\phi \cos 2\alpha \tag{2}$$

Then, the required parameters after the fitting can be derived by the following equation:

$$I_i = a_0 + a_1 \sin\alpha + a_2 \cos\alpha \tag{3}$$

By comparing equations (2) and (3), the parameters are obtained:

$$a_0 = \frac{1}{2} I_0, a_1 = \frac{1}{2} I_0 \sin\delta \cos 2\phi, a2 = -\frac{1}{2} I_0 \sin\delta \sin 2\phi \tag{4}$$

By rotating the polarization angle along a complete circumference with a resolution of 1°, a total number of angles N= 360° and a_0, a_1 and a_2 are calculated as:

$$a_0 = \sum_{i=1}^{N} \frac{1}{N} I_i, a_1 = \sum_{i=1}^{N} \frac{2}{N} I_i \sin\alpha_i, a_2 = \sum_{i=1}^{N} \frac{2}{N} I_i \sin\alpha_i \tag{5}$$

Using these parameters, the desired quantities can be found as:

$$I_{dp} = a_0, \sin\delta = \frac{(a_1^2 + a_2^2)^{\frac{1}{2}}}{a_0}, \phi = \frac{1}{2} \arccos\left(+ \frac{(a_1^2 + a_2^2)^{\frac{1}{2}}}{a_0} \right) \tag{6}$$

And then, Stokes parameters can be calculated by a mutual relationship between Jones and Muller model as follows:

$$\begin{aligned} S_0 &= I_{dp}(1+\sin\delta) = E_{0x}^2 + E_{0y}^2 \\ S_1 &= I_{dp}(1+\sin\delta)\cos 2\phi = E_{0x}^2 - E_{0y}^2 \\ S_2 &= 2\sqrt{I_{dp}}(1+\sin\delta)\cos 2\phi = 2E_{0x}E_{0y}\sin\delta \\ S_3 &= 2\sqrt{I_{dp}}(1+\sin\delta)\sin 2\phi = 2E_{0x}E_{0y}\cos\delta \end{aligned} \tag{7}$$

These Stokes parameters are calculated from the I_{dp}, $sin\delta$, and ϕ which are derived after the fitting and filtration process (Eq. (6)). For this reason, Stokes parameters measured with this method definitely will show extra sensing of sub-wavelength scattering as compared to those measured by the traditional method.

3. Results and Discussion

Stokes parameters of a Cu_2O spherical particle with a diameter of 900 nm are obtained by using a classical technique and PIMI method as displayed in Figure 4 (a) and (b), respectively. This particle has the interest of being able to support several resonant scattering modes in the visible range. That provides a sub-wavelength light confinement and a complex spatial distribution of Stokes parameters. In the classical method (Fig. 4(a)), the field distribution is not well resolved as it is compared with simulations (Fig. 4(c)). Results of S_0 to S_2 show an almost isotropic distribution without any angular information. On the other hand, S_3 shows a certain angular distribution, however the boundary of the Cu_2O sphere is not very clear.

The lost information can be observed by comparing these results with the theoretical calculation of the Stokes parameters by using a numerical method. In particular, FDTD numerical simulations have been carried out to obtain the Stokes parameters of the considered sample and are displayed in Fig. 4(c). It can be seen that the spatial distribution is quite complex with well-defined lobes, either inside or outside of the particle. In contrast with the conventional method, Fig. 4b shows the Stokes parameters images provided by PIMI. In this case, a complex distribution is observed, as expected and lobe distribution is in accordance with numerical simulations (Fig. 4c). In S_0, which represents the total intensity [38], the low and high intensity lobes are well resolved, both inside and outside the particle limits, as can be seen in Fig. 4(b). Although there is not a perfect matching between numerical simulations and PIMI image, the improvement from a conventional method is clearly observed and the quantity of information increases considerably. S_1 and S_2 parameters also delivered the angular distribution in a much better way as compared to the traditional method. S_3 parameter provides scattering difference under a left and right circularly polarized incident light [38]. This means that, in terms of S_3, we can get sub-wavelength information about the chirality from the PIMI system.

By comparing the spatial signature provided by our indirect Stokes parameters with FDTD calculations as displayed in Fig. 4(c), we can identify few mismatches, for instance in the center of the particle and also out of the particle boundaries. The reason may lie in the fact that in simulations, we sliced the particle through its center, whereas PIMI measurement considers their value in the surface. Despite this, the similarity in the scattering distribution of S_2 and S_3 is remarkable. The similarities in FDTD and PIMI spatial signature delivered by Stokes parameters proved that PIMI system having the capability to image the Stokes parameters with sub-diffraction far field distribution and an important improvement with respect to classical techniques.

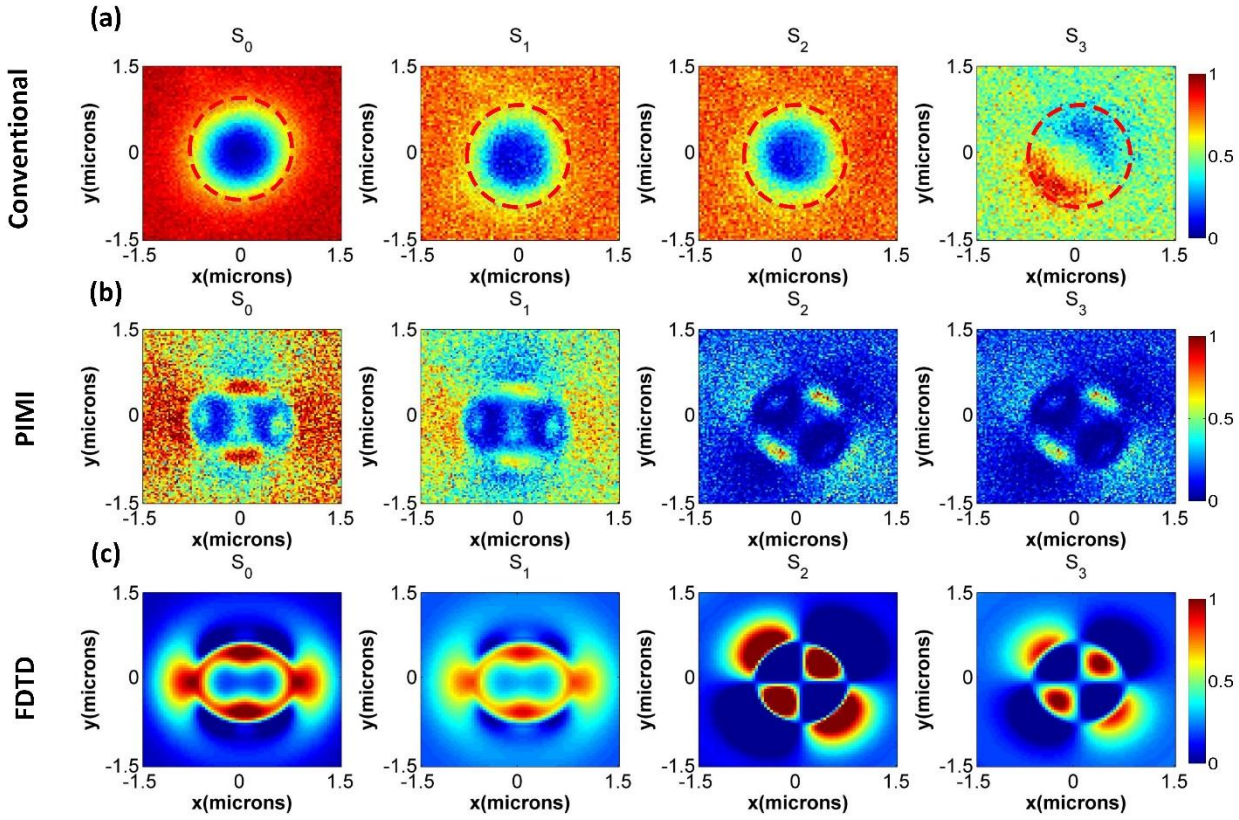

Figure 4. (a) Stokes parameter of a 900 nm Cu_2O submicron sphere measured with the conventional method under bright field illumination using a wavelength of 532 nm. (b) Stokes parameters delivered by PIMI method using the same measurement conditions as adopted in the traditional method. (c) FDTD calculated Stokes parameters.

Conclusion

We reported here a novel way to map the Stokes parameters of a submicron Cu_2O sphere with sub-wavelength information. We compared this spatial signature with the Stokes parameters delivered by the classical method. We found our Stokes parameters spatial signature contains finer details about sub-diffraction field distribution of SUT lacked by a conventional method. We proved the spatial scattering delivered by PIMI Stokes parameters by FDTD method.

Methods

Sample Preparation

For synthesizing the Cu_2O spherical particles, a typical solution route was applied. The research grade reagents were purchased from Sigma-Aldrich Company and used as it is in the experiment. In the first step, the transparent light green solution was prepared by slowly adding polyvinylpyrrolidone in *100 mL* $CuCl_2.2H_2O$ solution. After that 10 mL, sodium hydroxide (NaOH) was added into the *polyvinylpyrrolidone-*$CuCl_2.2H_2O$ solution and stir for 30 minutes. In the next step, ascorbic acid was added into *PVP-*$CuCl_2.2H_2O$ solution drop by drop and aged for 3 hours. These steps were performed in the water bath with constant stirring and heating. The molarities of polyvinylpyrrolidone, NaOH, and ascorbic acid were 0.01 mol L^{-1} (PVPMW 30000), 2.0 mol L^{-1} and 0.6 M respectively. The obtained solution was centrifuged to get the desired precipitate. After that several times, washing was performed with DI water and ethanol to get rid of impurities followed by drying in an oven for several hours [43].

Parametric Indirect Microscopic Imaging (PIMI)

PIMI system has been built by modifying the conventional microscopy Olympus BX51. An un-polarized visible source in the form of an incandescent lamp has been used. We have incorporated a homemade system in the optical path which is composed of a polarization modulation module with an angle precision of 0.05 degree and a Basler (PiA2400-17gm) CCD with a pixel resolution of 3.45 micron. The 3.45-micron-pixel CCD resolution leads to an outmost potential resolving power of 34.5nm if diffraction limit is broken and the Nyquist principle is fulfilled in the microscopic system, working with a 100x objective. The direct and indirect optical images were carried out at the illumination wavelength of 532nm.

Acknowledgement

The authors wish to acknowledge the financial support National Key Research and Development Program of China (2017YFF0107100), National Natural Science Foundation of China (NSFC) (61501239), NSFC-2017 (International Young Scientist Research Fund no. 61750110520) and the "Zijin Professor Project" of Nanjing University of Science and Technology. MH thanks the National Natural Science Foundation of China for financial support (Project nos. U1532112, 11375198, 11574280). BGC thanks the funding through the R&D Program SINFOTON S2013/MIT-2790 of the Comunidad de Madrid and from Agencia Estatal de Investigación (AEI) and Fondo Europeo de Desarrollo Regional (FEDER) for the Project TEC2016-77242-C3-1-R AEI/FEDER, UE.

References

[1] Lu D, Liu Z. Hyperlenses and metalenses for far-field super-resolution imaging. Nat Commun 2012;3:1205. doi:10.1038/ncomms2176.

[2] Hell SW, Wichmann J. Stimulated-Emission-Depletion Fluorescence Microscopy. Opt Lett 1994;19:780–2. doi:10.1364/OL.19.000780.

[3] Zheludev NI. What diffraction limit? Nat Mater 2008;7:420–2. doi:10.1038/nmat2163.

[4] Hell SW. Far-field optical nanoscopy. 2010 23rd Annu Meet IEEE Photonics Soc PHOTINICS 2010 2010;1153:3–4. doi:10.1109/PHOTONICS.2010.5698725.

[5] Sheppard CJR. Fundamentals of superresolution. Micron 2007;38:165–9. doi:10.1016/j.micron.2006.07.012.

[6] Mortensen KI, Churchman LS, Spudich JA, Flyvbjerg H. Optimized localization analysis for single-molecule tracking and super-resolution microscopy. Nat Methods 2010;7:377–81. doi:10.1038/nmeth.1447.

[7] Wong AMH, Eleftheriades G V. An Optical Super-Microscope for Far-field, Real-time Imaging Beyond the Diffraction Limit. Sci Rep 2013;3:1715. doi:10.1038/srep01715.

[8] Hirano Y, Matsuda A, Hiraoka Y. Recent advancements in structured-illumination microscopy toward live-cell imaging. Microscopy 2015;64:237–49. doi:10.1093/jmicro/dfv034.

[9] Hell SW, Sahl SJ, Bates M, Zhuang X, Heintzmann R, Booth MJ, et al. The 2015 super-resolution microscopy roadmap. J Phys D Appl Phys 2015;48:443001. doi:10.1088/0022-3727/48/44/443001.

[10] Rust MJ, Bates M, Zhuang XW. Sub-diffraction-limit imaging by stochastic optical reconstruction microscopy (STORM). Nat Methods 2006;3:793–5. doi:Doi 10.1038/Nmeth929.

[11] Montgomery PC, Leong-Hoi A, Anstotz F, Mitev D, Pramatarova L, Haeberlé O. From superresolution to nanodetection: overview of far field optical nanoscopy techniques for nanostructures. J Phys Conf Ser 2016;682:12010. doi:10.1088/1742-6596/682/1/012010.

[12] Small A, Stahlheber S. Fluorophore localization algorithms for super-resolution microscopy. Nat Methods 2014;11:267–79. doi:10.1038/nmeth.2844.

[13] Patterson G, Davidson M, Manley S, Lippincott-Schwartz J. Superresolution Imaging using Single-Molecule Localization. Annu Rev Phys Chem 2010;61:345–67. doi:10.1146/annurev.physchem.012809.103444.

[14] Yildiz A, Selvin PR. Fluorescence imaging with one nanometer accuracy: Application to molecular motors. Acc Chem Res 2005;38:574–82. doi:10.1021/ar040136s.

[15] Ober RJ, Ram S, Ward ES. Localization Accuracy in Single-Molecule Microscopy. Biophys J 2004;86:1185–200. doi:10.1016/S0006-3495(04)74193-4.

[16] Betzig E, Patterson GH, Sougrat R, Lindwasser OW, Olenych S, Bonifacino JS, et al. Imaging Intracellular Fluorescent Proteins at Nanometer Resolution. Science 2006;313:1642–5. doi:10.1126/science.1127344.

[17] Carney PS, Fischer DG, Foley JT, Friberg AT, Shchegrov A V, Visser TD, et al. Comment - Evanescent waves do contribute to the far field. J Mod Opt 2000;47:757–8. doi:10.1080/09500340008233395.

[18] Xiao M. Evanescent fields do contribute to the far field. J Mod Opt 1999;46:729–33. doi:10.1080/09500349908231298.

[19] Hao X, Kuang CF, Gu ZT, Wang YF, Li S a, Ku YL, et al. From microscopy to nanoscopy via visible light. Light Appl 2013;2:e108. doi:10.1038/lsa.2013.64.

[20] Rotenberg N, Kuipers L. Mapping nanoscale light fields. Nat Photonics 2014;8:919–26. doi:10.1038/nphoton.2014.285.

[21] Lewis A, Taha H, Strinkovski A, Manevitch A, Khatchatouriants A, Dekhter R, et al. Near-field optics: from subwavelength illumination to nanometric shadowing. Nat Biotechnol 2003;21:1378–86. doi:10.1038/nbt898.

[22] Neuman T, Alonso-González P, Garcia-Etxarri A, Schnell M, Hillenbrand R, Aizpurua J. Mapping the near fields of plasmonic nanoantennas by scattering-type scanning near-field optical microscopy. Laser Photonics Rev 2015;9:637–49. doi:10.1002/lpor.201500031.

[23] Bettiol AA, Mi Z, Watt F. High-resolution fast ion microscopy of single whole biological cells. Appl Phys Rev 2016;3:41102. doi:10.1063/1.4971414.

[24] Jacob Z, Alekseyev L V., Narimanov E. Optical Hyperlens: Far-field imaging beyond the diffraction limit. Opt Express 2006;14:8247. doi:10.1364/OE.14.008247.

[25] Lee H, Liu Z, Xiong Y, Sun C, Zhang X. Development of optical hyperlens for imaging below the diffraction limit. Opt Express 2007;15:15886. doi:10.1364/OE.15.015886.

[26] Wang W, Xing H, Fang L, Liu Y, Ma J, Lin L, et al. Far-field imaging device: planar hyperlens with magnification using multi-layer metamaterial. Opt Express 2008;16:21142. doi:10.1364/OE.16.021142.

[27] Wang YT, Cheng BH, Ho YZ, Lan Y-C, Luan P-G, Tsai DP. Gain-assisted hybrid-superlens hyperlens for nano imaging. Opt Express 2012;20:22953–60.

doi:10.1364/OE.20.022953.

[28] Zhang T, Chen L, Li X. Graphene-based tunable broadband hyperlens for far-field subdiffraction imaging at mid-infrared frequencies. Opt Express 2013;21:20888–99. doi:10.1364/OE.21.020888.

[29] M. Meier, V. Romano and TF. Material processing with pulsed radially and azimuthally polarized laser radiation. Appl Phys A 2007;86:329–34. doi:10.1007/s00339-006-3784-9.

[30] Osorio CI, Mohtashami A, Koenderink AF. K-space polarimetry of bullseye plasmon antennas. Sci Rep 2015;5:9966. doi:10.1038/srep09966.

[31] Chen W, Zhan Q. Realization of an evanescent Bessel beam via surface plasmon interference excited by a radially polarized beam. Opt Lett 2009;34:722–4. doi:10.1364/OL.34.000722.

[32] Marcatili EAJ, Schmeltzer RA. Hollow Metallic and Dielectric Waveguides for Long Distance Optical Transmission and Lasers. Bell Syst Tech J 1964;43:1783–809. doi:10.1002/j.1538-7305.1964.tb04108.x.

[33] Berry HG, Gabrielse G, Livingston AE. Measurement of the Stokes parameters of light. Appl Opt 1977;16:3200. doi:10.1364/AO.16.003200.

[34] Collett E. Measurement of the four Stokes polarization parameters with a single circular polarizer. Opt Commun 1984;52:77–80. doi:10.1016/0030-4018(84)90286-4.

[35] Rodríguez-Herrera OG, Lara D, Dainty C. Far-field polarization-based sensitivity to sub-resolution displacements of a sub-resolution scatterer in tightly focused fields. Opt Express 2010;18:5609–28. doi:10.1364/OE.18.005609.

[36] Qin F, Huang K, Wu J, Jiao J, Luo X, Qiu C, et al. Shaping a subwavelength needle with ultra-long focal length by focusing azimuthally polarized light. Sci Rep 2015;5:1–9. doi:10.1038/srep09977.

[37] Liu X, Qiu B, Chen Q, Ni Z, Jiang Y, Long M, et al. Characterization of graphene layers using super resolution polarization parameter indirect microscopic imaging. Opt Express 2014;22:20446. doi:10.1364/OE.22.020446.

[38] Collett E. Field Guide to Polarization (SPIE Vol. FG05). 2005.

[39] Phuoc GH, Pham THT. Measuring the stokes polarization parameters. IFMBE Proc 2018;63:593–6. doi:10.1007/978-981-10-4361-1_101.

[40] Trippe S. Polarization and polarimetry: A review. J Korean Astron Soc 2014;47:15–39. doi:10.5303/JKAS.2014.47.1.15.

[41] Glazer AM, Lewis JG, Kaminsky W. An automatic optical imaging system for birefringent media. Proc R Soc London Ser a-Mathematical Phys Eng Sci 1996;452:2751–65. doi: 10.1098/Rspa.1996.0145.

[42] Kaminsky W, Claborn K, Kahr B. Polarimetric imaging of crystals. Chem Soc Rev 2004;33:514–25. doi:10.1039/b201314m.

[43] Zhang DF, Zhang H, Guo L, Zheng K, Han XD, Zhang Z. Delicate control of crystallographic facet-oriented Cu2O nanocrystals and the correlated adsorption ability. J Mater Chem 2009;19:5220–5. doi:10.1039/b816349a.